Journal of King Saud University – Science 34 (2022) 101797

Contents lists available at ScienceDirect

Journal of King Saud University – Science

journal homepage: www.sciencedirect.com

Original article

A comparative cytotoxic study against breast cancer cells with nanoparticles and rods shaped structures

Abdulsalam A. Alkhudhayri

Department of Biology, College of Science, University of Hafr Albatin, Hafr Albatin 31991, Saudi Arabia

ARTICLE INFO

Article history:
Received 11 October 2021
Revised 18 December 2021
Accepted 21 December 2021
Available online 25 December 2021

Keywords:
Nanoparticle
Nanorods
MTT
NRU
ROS
MCF-7

ABSTRACT

The zinc oxide (ZnO) nanostructures are highly influential material and exhibit numerous properties. Numerous physicochemical applications for instance electronic, catalyst, solar cells, hydrogen fuels and energy evolution. Besides the large application in various directions very few reports are available for the cytotoxic evaluations and their compression with nano particles (NPs) and nanrorods (NRs) against the breast (MCF-7) cancer cells. The ZnO-NPs and NRs were produced through solution process in a short time span and were well characterized. The cells viability was tested with MTT and NRU assays. A series of different concentrations (2 μg/mL, 5 μg/mL, 10 μg/mL, 25 μg/ mL, 50 μg/mL, 100 μg/mL and 200 μg/mL) of NRs and NPs were employed against cancer cells for to evaluate the % activity of sustained and non-sustained cells. The morphology of treated and control cells were observed via microscopy respectively. Including this, the genetic studies were also scrutinized, cell-cycle analysis express the upsurge in the apoptotic peak after a 24-h. Quantitative PCR (qPCR) data revealed that the mRNA levels of apoptotic genes such as p53, bax, and caspase-3 were upregulated, whereas bcl-2, an anti-apoptotic gene, was downregulated; therefore, apoptosis was mediated through the p53, bax, caspase-3, and bcl-2 pathways.
© 2021 The Author. Published by Elsevier B.V. on behalf of King Saud University. This is an open access article under the CC BY-NC-ND license (http://creativecommons.org/licenses/by-nc-nd/4.0/).

1. Introduction

The size of nanostructures is an important parameter, which influences several characteristics such as physical, chemical, electronic, magnetic, quantum and various other properties. The nanostructures (NSs) are classified based to their dimensional (D) structures as 0D, 1D, 2D, where several types of structures can be formed by various physicochemical methods (Saleh, 2020, Khan et al., 2019). A number of different structures with shape and sizes are formed from different ways for instance, quantum dots (QDs), nanoparticles (NPs), nanorods (NRs), nanoflowers (NFs), microflowers (MFs), spheres, sea urchins and various others types were fabricated (Kim et al., 2019). These nano and micro structural (MSs) materials exhibit numerous properties, which enhanced their electronic, magnetic, chemical, optical and surface characteristics. It also fundamentally different from their corresponding atoms, molecules, catalysts, ferrofluids, storage, markers, chemical and biological sensors, imaging, pigments etc (Baek and Khang, 2020). A number of physical and chemical ways had been adopted to prepare different shaped structures such as plasma chemical vapor deposition, chemical vapor deposition, high temperature chemical vapor deposition, microwave, sputtering, flame assisted, Atomic layer deposition approach etc (Wahab et al., 2011a,b; Saeed et al., 2020., Beaudette et al., 2020, Gürsoy, 2020). The physical means are costly and it requires extensive care and infrastructures. Over various ways of preparation, solution process such as co-precipitation, hydrothermal, sol–gel etc; provides easier and cost effective ways, which needs less infrastructures and can produce a bulk amount with high thermal stability, durable and biocompatible property (Wahab et al., 2008) etc. With an ample oxides based nano and microstructures, the zinc oxide (ZnO) provides numerous structures and that's why it's so called bucket of nano and microstructures (Wahab et al., 2007). It's well documented that ZnO exhibit plentiful properties for instance enhanced surface area, high band gap energy (3.37 eV), thermodynamically stable with good mechanical strength (Wahab et al., 2007b). Due to versatile nature, it's largely applied in innumerable fields for instance catalyst, sensors, storage, lasers, detectors, solar cells, LEDs, optoelectronics (Ahamed et al., 2021a,b, Wibowo et al., 2020, Theerthagiri et al., 2019) etc. Additionally, the chemically synthesized ZnO also exhibit a biocompatible nature for biological

E-mail address: alkhudhayri@uhb.edu.sa
Peer review under responsibility of King Saud University.

Production and hosting by Elsevier

https://doi.org/10.1016/j.jksus.2021.101797
1018-3647/© 2021 The Author. Published by Elsevier B.V. on behalf of King Saud University.
This is an open access article under the CC BY-NC-ND license (http://creativecommons.org/licenses/by-nc-nd/4.0/).

materials (Rajashekara et al., 2020). The ZnO allows in different biological objects such as DNA (Wahab et al., 2009), drug delivery (Martínez-Carmona et al., 2018), cancer, bacterial and others studies etc (Wiesmann et al., 2020). Although, a number of applications of nanostructures but limited studies are available in the area of cancer research with nanostructure and have many rooms to do more and more work (Ijaz et al., 2020). As it's well-known that the cancer is a denying disease, which spreads with the abnormal growth of normal cells. Towards to this direction, the NSs toxicity with ZnO was studies with different cell lines such as yeast accharomyces cerevisiae with defined mechanism of mechanical damage (Márquez et al., 2018) were studied. In other work, the dissimilar geometrical nanostructures were utilized as a dose dependent against brain tumor (U87), cervical (HeLa) and normal HEK cells, which showed the effectiveness of NSs (Wahab et al., 2013). It's well documented that oxide based NSs and MSs exhibit good effect on various cells and related entities but the cost is again a matter to handle these issues (Wahab et al., 2013). Although a number of research work published to this direction and shows the applicability of NPs with different cell lines but very limited reports are available which show the application of altered shaped structures against cancer cells (Ijaz et al., 2020, Wahab et al., 2013).

The present work described the utility of NPs and compared it with the NRs against toxicity studies processed via solution process. The synthesized powder were analyzed via several instruments such as XRD, FESEM and FTIR respectively. The cells interactions with NSs were examined via microscope whereas the cancer cells viability with and without NSs were confirmed from the MTT and NRU. The apoptosis in cells were observed via mRNA expression with genes including control with NPs and NRs.

2. Experimental

2.1. Material and methods

2.1.1. Synthesis of NPs and NRs through solution process

2.1.1.1. Nanoparticles (NPs). The production of zinc oxide nanoparticles (NPs) were accomplished with the use of zinc nitrate hexa hydrate ($Zn(NO_3)_2{\cdot}6H_2O$), which act as a precursor material, whereas sodium hydroxide and propyl amine were used as reducing agent (Wahab et al., 2011b) with small modification. For the synthesis of NPs, zinc salt ($Zn(NO_3)_2{\cdot}6H_2O$), 0.35 M) were dissolved in methanol (MeOH) under constant starring. Once the zinc salt completely dissolved, ~ 20–25 mL of propyl amine was added slowly slowly and observes the colour of the solution, which shows no change in the solution. A small amount of sodium hydroxide (NaOH, 0.1 M) was added to this solution and examined the pH value, which exceeds up to 12.5. A small flocculation was appeared in the beaker for a few seconds (*s*) and disappeared. The mixture was transferred in a refluxing pot and refluxed it at 65 °C for 6 h. Initially, no precipitation was observed, whereas once the refluxing temperature reaches to their optimized value, the initial nuclei of particles were form at the bottom of refluxing pot. When the refluxing time was completed, white colored precipitate was collected and washed via centrifugation at 3000 rpm/3min (Eppendorf, 5430R, Centrifuge, Germany) and dried. The recovered powder was further analysed via various characterizations tools.

2.1.1.2. Nanorods (NRs). The NRs were synthesised with as per the previously reported work with slight alternation (Wahab et al., 2011a). For the synthesis of NRs, zinc acetate dihydrate ($Zn(Ac)_2{\cdot}2H_2O$) was applied as a prime precursor and NaOH was utilized as a directing agent. A small amount of $Zn(Ac)_2{\cdot}2H_2O$ (0.3 M) was dissolved in 100 mL of double distilled water under constant stirring. Afterword's, in this solution NaOH (0.2 M) was mixed gently and pH (Cole Parmer U.S.A) of the solution was measured and its upsurge to 12.7. The solution was moved to refluxing pot and heated to the solution for 60 min at 90 °C. The powdery solution was collected in a refluxing pot, washed with alcohol and centrifuged at 3000 rpm/3 min and dried.

2.1.2. Characterizations

The X-ray diffraction pattern (XRD) was utilized to observe the crystallinity of the prepared powder, particle size, phases etc. The powder samples were examined between 20 and 80° with using $Cu_{K\alpha}$ radiation (λ = 1.54178 Å) at 6°/min scanning speed with 40 kV voltage and 30 mA current. The morphological characteristics were examined with FESEM (Hitachi, Japan). The chemical characteristics of powder samples were accessed via FTIR ranges from 400 to 4000 cm^{-1} using potassium bromide powder (KBr) pellets, fixed it with sample holder and characterized the material.

2.2. Cell culture (MCF-7 cells) and exposure with NPs and NRs

The breast cancer cells (MCF-7) was grown in a medium DMEM with 10% fetal bovine serum (FBS), 0.2% sodium bicarbonate, and antibiotic–antimycotic solution (100 X, 1mL/100 mL) with moist environment (5% CO_2 & 95% O_2) at 37 °C. Earlier for the experiments, the cells viability were evaluated by trypan blue dye as per the protocol (Siddiqui et al., 2008) and shown the viability more than 95% were only used in the study. The cells were employed between 10 and 12 passages to treat the cells with NSs. The NPs and NRs were used at high concentration and then subsequently diluted at desired different concentrations for the exposure of cells. The cells were plated in 6-well or 96-well plates as per the experimental requirement.

2.3. Reagents and consumables for the biological study

The MTT [3-(4, 5-dimethylthiazol-2-yl)-2, 5 diphenyltetrazolium bromide], was recovered from Sigma Chem.Co.USA and castoff without any further modification except dilution, besides this the Dulbecco's Modified Eagle Medium (DMEM) and MEM culture medium, antibiotics-antimycotic and FBS were bought from Invitrogen, USA. The plastic wares and other consumables products for cells culture were used from Nunc, Denmark.

2.4. MTT assay

Cancer cells viability with (treated) and without NPs and NRs (control) were accessed via MTT assay as per the previous followed protocol (Mosmann 1983). Initially, cells were cultured in a specialized 96 well plates (rate of 1×10^4/well) with permissible to follow for 24 h at 37 °C with humidified environment. The cells were intermingled with NPs and NRs from 2 to 200 μg/mL for 24 h. When the cells were completely inter mixed in well plates, stock solution of MTT (5 mg/mL in PBS) was amalgamated with rate of 10 μL/well in 100 μL of cell suspension and further incubated for 4 h. After the completion of incubation period, the well plate's solution was with draw from the pipette and in these wells ~ 200 μL of DMSO was added for to aspirate the formazan product and assorted gently. The optical characteristic of the solution was analyzed at 550 nm with micro-plate reader (Multiskan Ex, Thermo Scientific, Finland). The control cells were also employed as a reference and to run with the same conditions. The value of maximum absorbance depends upon the employed solvent in sample solution and level of viability of cells % was calculated as per the equations mentioned below:

$$\%\ viability = [(total\ cells - viable\ cells)/total\ cells] \times 100$$

2.5. NRU assay

The cytotoxic assessment was also confirmed with and without NPs and NRs via NRU assay as per the previously described procedure (Siddiqui et al., 2010, Borenfreund and Puerner, 1985). The MCF-7 cells (1×10^4/well) cells were sowed in a specified 96 well plates. Once the cells were completely grown (after 24 h) were exposed to desired conc (2–200 μg/mL) of NPs and NRs and kept for 24 h in an incubator. When the exposure was completed, cells were further incubated in NRs medium (100 μg/mL) for 3 h. Thereafter, cells were cleaned and dye was extracted in 1% acetic acid and 50% ethanol solution. The develop color was read at 540 nm.

2.6. RNA isolation and qPCR analysis of apoptotic marker genes

The RNA isolation was performed with cultured cells of MCF-7 cells in a 6-well plates control and treated sample of NPs and NRs at concentration of 50 μg/mL for 24 h. The RNA was mined from RNeasy mini Kit (Qiagen) as according to manufacturer's protocol. The cDNA was synthesized from treated and untreated cells taking 1 μg of RNA by Reverse Transcriptase kit using MLV reverse transcriptase (GE Health Care, UK) as per the manufactures' protocol. The RT-PCR was performed on Roche® Light Cycler®480 (96-well block) (USA) following the cycling program recommended. 2 μL (40 ng) of cDNA template included the 20 μL volume to this reaction mixture (Ahmad et al., 2020).

3. Results and discussion

3.1. X-ray diffraction pattern (XRD)

The synthesized white powders were examined through XRD, and it defines the crystallite size, phases and crystallinity of the processed powder. The obtained spectra's (Fig. 1.) of both powder shows that the indexed and assign peaks with their related positions such as ⟨100⟩ (31.65), ⟨002⟩ (34.35), ⟨101⟩ (36.30), ⟨102⟩ (47.40), ⟨110⟩ (56.50), ⟨103⟩ (62.80), ⟨200⟩ (66.15), ⟨112⟩ (67.85), ⟨201⟩ (69.01), ⟨004⟩ (72.25) and ⟨202⟩ (77.05), which are very closely represents the formation of ZnO with their lattice constants a = 3.249 Å and c = 5.206 Å, and very close to the Joint Committee on Powder Diffraction Standards (JCPDS 36–1451) data. The assign peaks such as ⟨100⟩ (31.65), ⟨002⟩ (34.35), ⟨101⟩ (36.30) in the spectrum illustrates that the dimension and phase of ZnO is wurtzite phase. From the XRD, phases, peaks positions, FWHM, crystallite size (nm) and average diameter of crystallite size (nm) were also calculated with well-known scherrer formula (Wahab et al., 2007a,b).

$$D = \frac{0.9\lambda}{\beta cos\theta} \quad (1)$$

In this equation λ is the wavelength of X-ray radiation source, β is full-width at half-maximum in [FWHM] radians, θ is Bragg's diffraction angle. The average value of particle size is ∼12 nm. The major sharp and intense peaks indicate that the synthesized powder particles exhibit good crystallinity, whereas FWHM defined that the size of each crystallite is very small. The rod shaped structures exhibit the average value of particle size is ∼25 nm. In the spectrum, no any chemical impurities were seen, again confirm that the powders are pure and wurtzite phase of ZnO nanosized material.

3.2. Morphological assessment

The morphological examination for the synthesized powders was accessed via FESEM and recovered images are displayed as Fig. 2(a-b). The received image (Fig. 2a) shows that number of spherical shaped structures are seen, which are in grouped. The shapes of the grown particles are in spherical, very minute in size, connected with other particles. The average particle diameter ranges from 12 to 15 nm (Wahab et al., 2008). Another image (Fig. 2b), represent the formation of perfectally grown rod shaped hexagonal structures. The surfaces are very clean, smooth and aligned. Once checked in detail the average diameter of each rod is in the range of 175–200 nm whereas the length of each rod exhi-

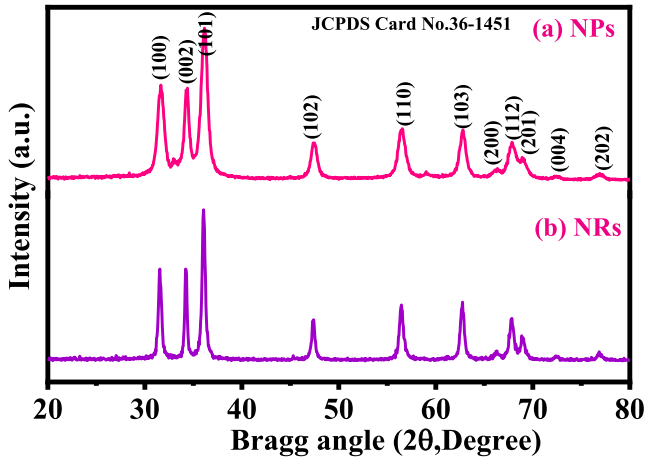

Fig. 1. Shows the X-ray diffraction pattern of NPs (a) and NRs (b).

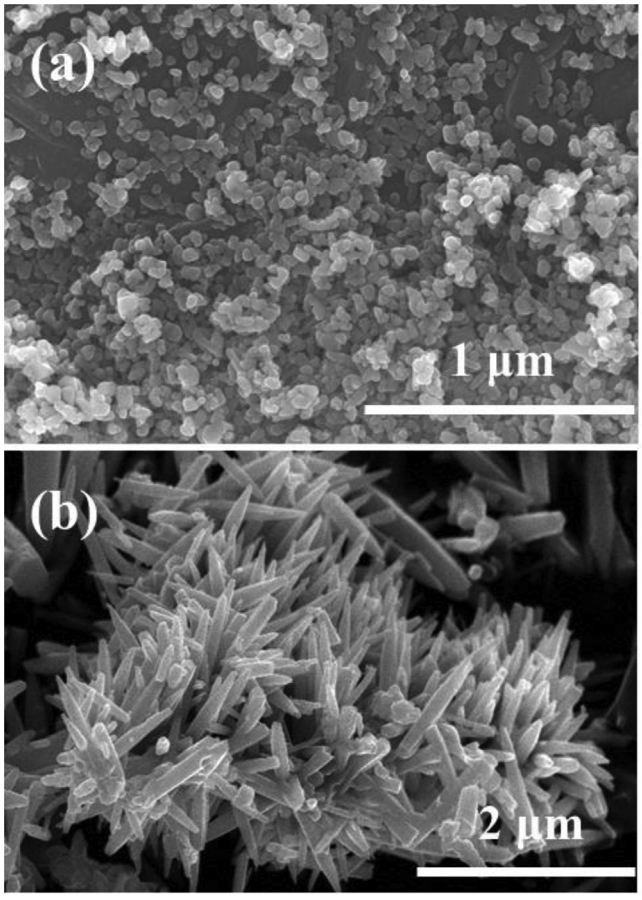

Fig. 2. Displayed FESEM images of synthesized NPs (a) and NRs (b) respectively.

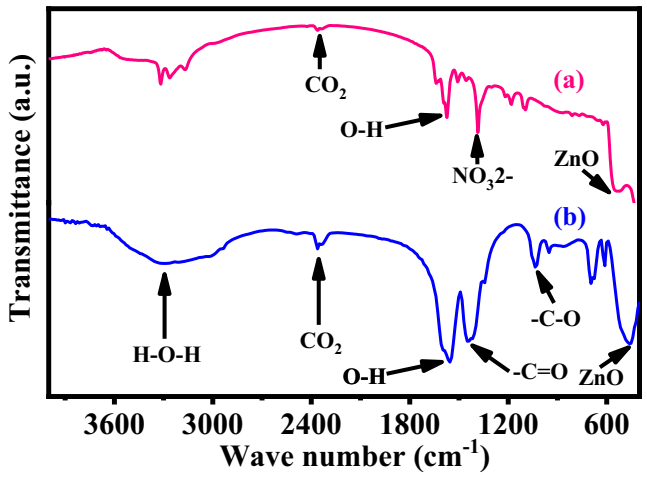

Fig. 3. Show the typical FTIR spectra of grown NPs (a) and NRs (b) respectively.

bit about 1.5–2 μm range. The rods are gathered together and form a bunched of nanostructures.

3.3. FTIR spectroscopy

The details of chemical functional groups in processed nano structural material were examined via FTIR spectroscopy and graphs are shown as Fig. 3. The major peak obtained in the FTIR spectrum between 3200 and 3600 cm^{-1} resembles to the H_2O whereas the asymmetric stretching mode of O–H water molecules are centered at 1576 and 1546 cm^{-1} (Fig. 3a-b) respectively. The peak at 2340 cm^{-1} is related to the CO_2 in the spectrum. The sharp peak is associated at 1384 and 1450 cm^{-1} related to the nitrate and acetate molecule (-C=O) (Wahab et al., 2008, Wahab et al., 2007a,b) respectively. Besides these, the sharp peak centered at 1035 cm^{-1} and 1042 cm^{-1} are the stretching and bending mode of (-C-O) and (NO_3^{2-}) correspondingly, whereas the 538 and 466 cm^{-1} represent the formation of ZnO in FTIR spectrum. The FTIR authenticates the formation of powder of NPs and NRs, and are closely consistent with the XRD pattern and FESEM.

3.4. Microscopic observations of cancer cells (MCF-7) with NPs and NRs

The breast cancer (MCF-7) cells were cultured as detailed in the material and method section and their morphological evaluation was examined via microscopy at 24 h incubation periods with a varied range of concentrations of NPs (Fig. 4a) and NRs (Fig. 4b) (2 μg/mL, 5 μg/mL, 10 μg/mL, 25 μg/mL, 50 μg/mL, 100 μg/mL and 200 μg/mL) with control (Fig. 4). From the recovered images, it's seems that there is no noteworthy change was observed at initial range of concentration (2 μg/mL, 5 μg/mL, 10 μg/mL) of NPs and NRs, but as the concentration was rises to 100 μg/mL, the cells growth was much influenced. At highest concentration of NPs and NRs (100 μg/mL and 200 μg/mL) the cells growth was much affected and morphology of cells was destroyed (Fig. 4). The images displayed that the cells (MCF-7) were damaged with the processed NPs and NRs (Fig. 4a and b). In this condition it also shows that the NPs damaged more cancer cells as compared with NRs.

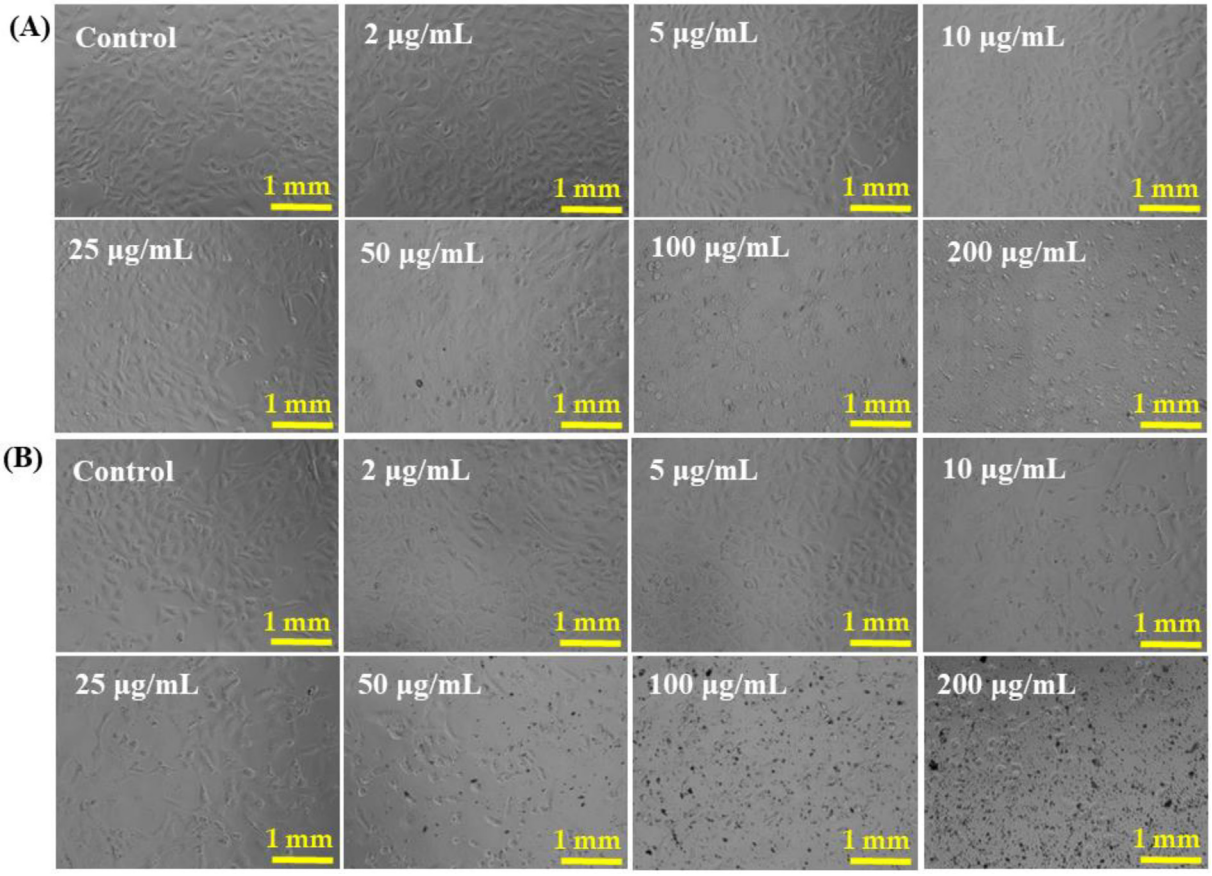

Fig. 4. The cells structural morphology of MCF-7 cells, exposed to different concentrations (2–200 μg/ml) of NPs (Panel A) and NRs (Panel B) for 24 h. Images were taken at 20x magnification. Scale bar = 1 mm.

3.5. The cytotoxicity assessment (MTT and NRU Assay) with NPs and NRs

The cytotoxicity (MCF-7 cells) was examined via MTT assay as detailed above with NPs and NRs from 2 to 100 μg/ml for 24 h incubation. The achieved result shows that viability of cancer cells were diminished with NPs and NRs and the data were dose-dependent. The MCF-7 cells viability for NPs, with MTT assay was diminutions at 24 h, 110%, 105%, 90%, 68%, 63%, 50% and 20% (Fig. 5A) at concentrations of 2, 5, 10, 25, 50 100 and 200 μg/mL respectively ($p < 0.05$ for each). The results were obtained with three independent experiments and expressed as the mean ± S.D.

Including the MTT assay the very similar observations were also observed in NRU assays of with NPs of cancer cells as described above. At initial concentration with cancer cells not much affected, whereas once the concentration or doses of NPs increases, cells were dimini-shed. The NPs were exposed with MCF-7, the NRU assay was decreases at 24 h, 108%, 109%, 102%, 98%, 88%, 60% and 24% (Fig. 5B) for the concentrations of 2, 5, 10, 25, 50, 100 and 200 μg/mL respectively ($p < 0.05$ for each). The results were obtained with three independent experiments and expressed as the mean ± S.D.

In case of NRs, the viability accessed with MTT assay was decreases at 24 h, 103%, 94%, 84%, 65%, 56%, 50% and 47% (Fig. 6A) for the concentrations of 2, 5, 10, 25, 50 100 and 200 μg/mL with control (100%) respectively ($p < 0.05$ for each). It reveals from the obtained data that initially NRs not affected whereas once the concentration raises the cytotoxicity of cancer cells were much influenced. In case of NRs exposed with MCF-7, the NRU assay was decreases at 24 h, 101%, 100%, 98%, 90%, 68%, 59% and 54% (Fig. 6B) for the concentrations of 2, 5, 10, 25, 50, 100, 200 μg/mL with control (100%) respectively ($p < 0.05$ for each). From the obtained data it reveals that the NPs are more effective as compared with NRs for the longer concentration range. The results were obtained and expressed as the mean ± S.D. of three independent experiments.

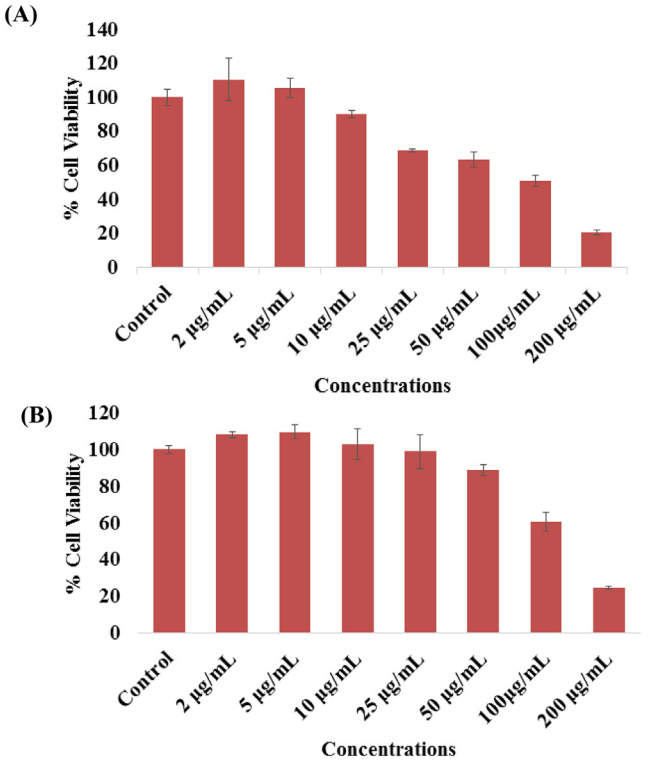

Fig. 5. The cytotoxicity assessment of NPs in MCF-7 cell line by MTT (A) and NRU (B) assays. Cells were exposed to different concentrations (2–200 μg/ml) of NPs for 24 h. Results are expressed as the mean ± S.D. of three independent experiments with statistical standard error ($p < 0.05$ for each).

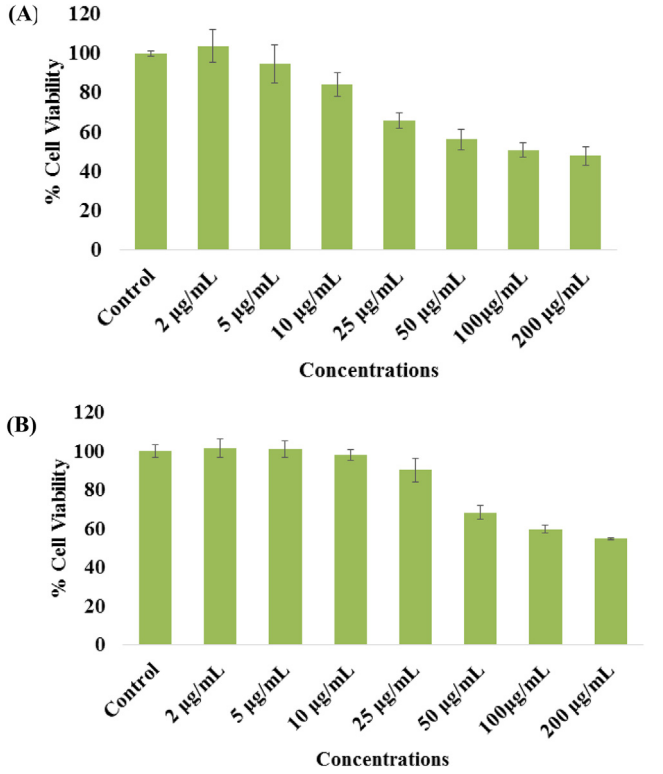

Fig. 6. The cytotoxicity assessment of NRs in MCF-7 cell line by MTT (A) and NRU (B) assays. Cells were exposed to different concentrations (2–200 μg/ml) of NRs for 24 h. Results are expressed as the mean ± S.D. of three independent experiments with statistical standard error ($p < 0.05$ for each).

3.6. Real time PCR induced by NPs and NRs

The mRNA levels for genes were also studied with using the qPCR. For this the breast cancer cells were treated to NPs (Fig. 7A) and NRs (Fig. 7B) for 24 h at a concentration of 100 μg/mL and qPCR was performed to evaluate the mRNA level of genes (p53, bax, casp3, and bcl-2). Significant changes were observed for the apoptotic genes in MCF-7 cells ($p < 0.05$ for each gene). The mRNA levels of tumor suppressor gene p53 and pro-apoptotic gene bax were upregulated. Additionally, it's also examined that the caspase-3 gene express higher in NPs treated with cells. The expression of bcl-2, an anti-apoptotic gene, was downregulated in cells treated with NRs (Fig. 7).

3.7. Discussion

In this study, we have prepared two different shaped nanostructures (NPs and NRs) of ZnO with a defined size 12–15 nm (NPs), whereas the NRs structures exhibit 200 nm diameter and length goes to 1.5–2 μm. The main objective of current study was to examine the cytotoxic responses of NPs and NRs against breast (MCF-7) cancer cells. The MTT assay was employed to check the cytotoxicity against cancer cells at 24 h with NPs and NRs. For the assessment of the viability of cancer (MCF-7) cells against the processed material a long range (2, 5, 10, 25, 50, 100 and 200 μg/mL) of NPs and NRs chosen and exposed for 24 h, which

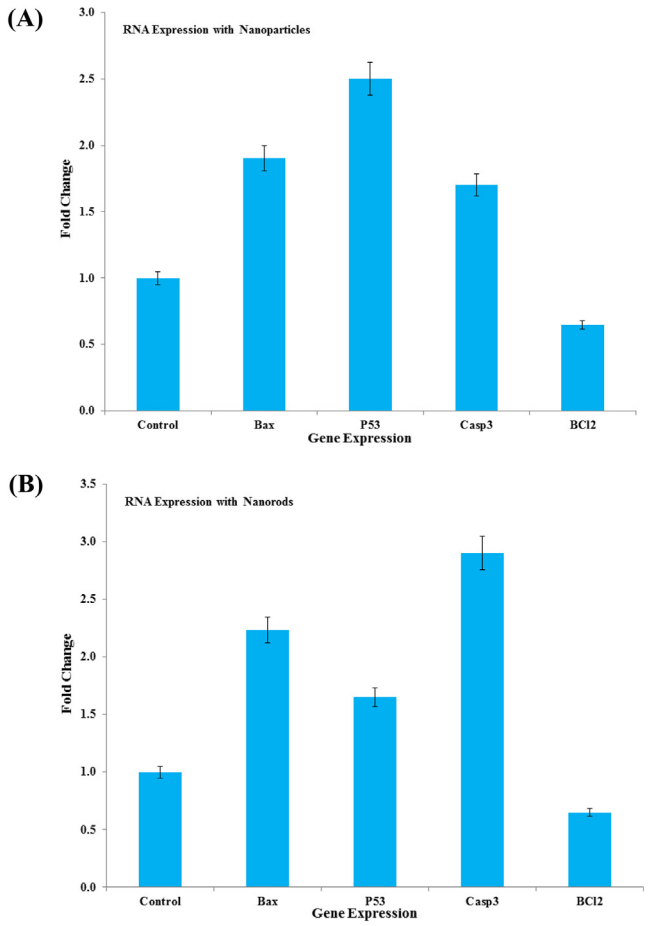

Fig. 7. mRNA quantification levels, fold change of apoptotic genes (p53, bax, and casp3) and anti-apoptotic gene (bcl-2) was analyzed. Cells treated 100 μg/mL of NPs (A)) and NRs (B) for 24 h. For the normalization an internal control of GAPDH used. The values are mean ± SE of three independent experiments with statistical standard error ($p < 0.05$ for each).

shows that viability cells were in concentration/dose dependent (Siddiqui et al., 2015). It's evident from the MTT assay that the viability of cells with NPs is much effective as compared with NRs. At initial not much effect was evident but as the concentration or doses of nanostructures were increase, the cytotoxicity was much affected. It's evident from the previous literature (Olejnik et al., 2020) that the shape and size of the nanostructures have possibility to produce reactive oxygen species (ROS) in cells suspension, which is an important factor and are responsible to form the free radicals (FRs) (Singh et al.,2020). The FRs in cells with NSs produces an enzymatic change, which resulted a disorder of the cells also to their contents and suggests that its extreme ROS generation reduces cells antioxidant capacity (Wahab et al., 2014, Hussain et al., 2009). The study summarizes that the cell death was induced with interaction of NPs, NRs and enhanced ROS generation, once treated with nanostructures. The obtained results are in accordance with the previously published literature on cytotoxic activity (Hussain et al., 2009). Also hypothesize that the cytotoxic activity of cancer cells were much influenced upon their unique structural geometry, distinctive property; functions are well responsible for the cell death. The data's showed that the nanostructures (NPs and NRs) exhibit potential against cancer cells growth inhibition, the results are based to their different concentrations, geometry of the NSs and are being able to enter easily to cells structures. The literature document reveals that researchers had employed NSs either for selected concentrations or opted at high concentrations for toxicity studies, may be damaging for human exposure (Hussain and Schlager, 2009; Hussain et al., 2009). Its consider that the NSs such as NPs and NRs and exhibit bio compatible materials that at lower conc. would be more and more obliging to control the growth of cancer cells and doesn't leave any hostile effect on the body.

4. Conclusion

The present work summarizes that the two different shaped ZnO nanostructures were processed and applied for to know the efficacy against breast cancer cells and characterized. The NPs and NRs were employed against breast cancer cells to check their efficacy of the material at different doses/ concentrations. The cells morphology of cancer cells (MCF-7) was studied via microscopy, which reveals that NPs and NRs express an effective dose dependent effect on cancer cells. The cells viabilities were measured via MTT and NRU assays and the results showed that NPs are much effective against cancer cells as compared to the NRs. The NPs and NRs exhibit enough capability to enter easily in cells and damaged their internal structures. It provides outstanding results to eradicate cancer cells as equated to the current technologies without any harmful effects. The NPs and NRs have possibility to make a passage to enter easily and quickly to the internal structures of cancer cells reduces the rate of growth of cancer cells as compared to other organic based drugs for cancer cells.

Declaration of Competing Interest

The authors declare that they have no known competing financial interests or personal relationships that could have appeared to influence the work reported in this paper.

References

Ahmad, J., Wahab, R., Siddiqui, M.A., Saquib, Q., Al-Khedhairy, A.A., 2020. Cytotoxicity and cell death induced by engineered nanostructures (quantum dots and nano particles) in human cell lines. J. Biol. Inorg. Chem. 25 (2), 325–338.
Ahamed, M., Akhtar, M.J., Khan, MA.M., Alhadlaq, H.A., 2021a. SnO_2-doped ZnO/reduced graphene oxide nanocomposites: synthesis, characterization, and improved anticancer activity via oxidative stress pathway. Inter. J. Nanomed 16, 89–104.
Ahamed, M., Akhtar, M.J., Khan, M.A., Alhadlaq, H.A., 2021b. A novel green preparation of Ag/RGO nanocomposites with highly effective anticancer performance. Polymers 13 (19), 3350.
Baek, S.E., Khang, D.Y., 2020. Selective growth of ZnO nanorods by thickness contrast in In-doped ZnO quantum dots seed layer. Nanotechnology 32, 055602.
Beaudette, C.A., Held, J.T., Mkhoyan, K.A., Kortshagen, U.R., 2020. Nonthermal plasma-enhanced chemical vapor deposition of two-dimensional molybdenum disulfide. ACS Omega 5 (34), 21853–21861.
Borenfreund, E., Puerner, J.A., 1985. Toxicity determined in vitro by morphological alterations and neutral red absorption. Toxicol. Lett 24 (2-3), 119–124.
Gürsoy, M., 2020. Fabrication of poly(N-isopropylacrylamide) with higher deposition rate and easier phase transition by initiated plasma enhanced chemical vapor deposition. Plasma Chem. Plasma Process. 40, 1063–1079.
Hussain, S.M., Schlager, J.J., 2009. Safety evaluation of silver nanoparticles: inhalation model for chronic exposure. Toxicol. Sci. 108, 223–224.
Hussain, S.M., Braydich-Stolle, L.K., Schrand, A.M., Murdock, R.C., Yu, K.O., Mattie, D. M., Schlager, J.J., Terrones, M., 2009. Toxicity evaluation for safe use of nano materials: recent achievements and technical challenges. Adv. Mater. 21 (16), 1549–1559.
Ijaz, M., Zafar, M., Islam, A., Afsheen, S., Iqbal, T., 2020. A review on antibacterial properties of biologically synthesized zinc oxide nanostructures. J. Inorg. Organometal. Polymers Mater. 30, 2815–2826.
Khan, I., Saeed, K., Khan, I., 2019. Nanoparticles: properties, applications and toxicities. Arab. J. Chem. 12 (7), 908–931.
Kim, K.S., Zakia, M., Yoon, J., Yoo, S.I., 2019. Metal-enhanced fluorescence in polymer composite films with Au@Ag@SiO2 nanoparticles and InP@ZnS quantum dots. RSC Adv. 9 (1), 224–233.
Márquez, I.G., Ghiyasvand, M., Massarsky, A., Babu, M., Samanfar, B., Omidi, K., Moon, T.W., Smith, M.L., Golshani, A., Mishra, Y.K., 2018. Zinc oxide and silver nanoparticles toxicity in the baker's yeast, Saccharomyces cerevisiae. PLoS One 13 (3), e0193111.

Martínez-Carmona, M., Gun'ko, Y., Vallet-Regí, M., 2018. ZnO nanostructures for drug delivery and theranostic applications. Nanomaterials 8 (4), 268.
Mosmann, T., 1983. Rapid colorimetric assay for cellular growth and survival: application to proliferation and cytotoxicity assays. J. Immunol. Methods 65 (1-2), 55–63.
Olejnik, M., Kersting, M., Rosenkranz, N., Loza, K., Breisch, M., Rostek, A., Prymak, O., Schürmeyer, L., Westphal, G., Köller, M., Bünger, J., Epple, M., Sengstock, C., 2020. 2020, Cell-biological effects of zinc oxide spheres and rods from the nano- to the microscale at sub-toxic levels. Cell Biol. Toxicol. 37 (4), 573–593. https://doi.org/10.1007/s10565-020-09571-z.
Rajashekara, S., Shrivastava, A., Sumhitha, S., Kumari, S., 2020. Biomedical applications of biogenic zinc oxide nanoparticles manufactured from leaf extracts of Calotropis gigantea (L.) Dryand. BioNanoScience 10, 654–671.
Saeed, M., Alshammari, Y., Majeed, S.A., Nasrallah, E.A., 2020. Chemical vapour deposition of graphene—synthesis, characterisation, and applications: a review. Molecules 25 (17), 3856.
Saleh, T.A., 2020. Nanomaterials: classification, properties, and environmental toxicities. Environ. Technol. Innovat. 20, 101067.
Siddiqui, M.A., Singh, G., Kashyap, M.P., Khanna, V.K., Yadav, S., Chandra, D., Pant, A. B., 2008. Influence of cytotoxic doses of 4-hydroxynonenal on selected neuro transmitter receptors in PC-12 cells. Toxicol. In Vitro. 22 (7), 1681–1688.
Siddiqui, M.A., Kashyap, M.P., Kumar, V., Al-Khedhairy, A.A., Musarrat, J., Pant, A.B., 2010. Protective potential of trans-resveratrol against 4-hydroxynonenal induced damage in PC12 cells. Toxicol. In Vitro 24 (6), 1592–1598.
Siddiqui, M.A., Saquib, Q., Ahamed, M., Farshori, N.N., Ahmad, J., Wahab, R., Khan, S. T., Alhadlaq, H.A., Musarrat, J., Al-Khedhairy, A.A., Pant, A.B., 2015. Molybdenum nanoparticles-induced cytotoxicity, oxidative stress, G2/M arrest, and DNA damage in mouse skin fibroblast cells (L929). Colloids Surf. B: Biointerfaces 125, 73–81.
Singh, R., Cheng, S., Singh, S., 2020. Oxidative stress mediated genotoxic effect of zinc oxide nanoparticles on *Deinococcus radiodurans*. 3 Biotech 10, 66.
Theerthagiri, J., Salla, S., Senthil, R.A., Nithyadharseni, P., Madankumar, A., Arunachalam, P., Maiyalagan, T., Kim, H.-S., 2019. A review on ZnO nanostructured materials: energy, environmental and biological applications. Nanotechnology 30 (39), 392001.
Wahab, R., Hwang, I.H., Kim, Y.-S., Shin, H.-S., 2011a. Photocatalytic activity of zinc oxide micro-flowers synthesized via solution method. Chem. Engg. J. 168 (1), 359–366.
Wahab, R., Hwang, I.H., Kim, Y.-S., Musarrat, J., Siddiqui, M.A., Seo, H.K., Tripathy, S. K., Shin, H.S., 2011b. Non-hydrolytic synthesis and photo-catalytic studies of ZnO nanoparticles. Chem. Engg. J 175, 450–457.
Wahab, R., Ansari, S.G., Kim, Y.S., Dar, M.A., Shin, H.-S., 2008. Synthesis and characterization of hydrozincite and its conversion into zinc oxide nanoparticles. J. Alloys Compounds 461 (1-2), 66–71.
Wahab, R., Ansari, S.G., Kim, Y.S., Seo, H.K., Kim, G.S., Khang, G., Shin, H.-S., 2007a. Low temperature solution synthesis and characterization of ZnO nano-flowers. Mater. Res. Bull. 42 (9), 1640–1648.
Wahab, R., Ansari, S.G., Kim, Y.-S., Seo, H.-K., Shin, H.-S., 2007b. Room temperature synthesis of needle-shaped ZnO nanorods via sonochemical method. Appl. Surf. Sci. 253 (18), 7622–7626.
Wahab, R., Kim, Y.-S., Hwang, I.H., Shin, H.-S., 2009. non-aqueous synthesis, characterization of zinc oxide nanoparticles and their interaction with DNA. Synthetic Metals 159, 2443–2452.
Wahab, R., Kaushik, N.K., Kaushik, N., Choi, E.H., Umar, A., Dwivedi, S., Musarrat, J., Al- Khedhairy, A.A., 2013. ZnO nanoparticles induces cell death in malignant human T98G gliomas, KB and non-malignant HEK cells. J. Biomed. Nanotechnol. 9, 1181–1189.
Wahab, R., Siddiqui, M.A., Saquib, Q., Dwivedi, S., Ahmad, J., Musarrat, J., Al-Khedhairy, A.A., Shin, H.S., 2014. ZnO nanoparticles induced oxidative stress and apoptosis in HepG2 and MCF-7 cancer cells and their antibacterial activity. Colloids Surf. B: Biointerfaces 117, 267–276.
Wibowo, A., Marsudi, M.A., Amal, M.I., Ananda, M.B., Stephanie, R., Ardy, H., Diguna, L.J., 2020. ZnO nanostructured materials for emerging solar cell applications. RSC Adv. 10, 42838–42859.
Wiesmann, N., Tremel, W., Briegera, J., 2020. Zinc oxide nanoparticles for therapeutic purposes in cancer medicine. J. Mater. Chem. B 8, 4973–4989.